

Catalytic effects on carbon/carbon composites fabricated by a film boiling chemical vapor infiltration process

H. Okuno, M. Trinquécoste, and A. Derré
CRPP/CNRS, Avenue Dr Albert Schweitzer, 33600 Pessac, France

M. Monthieux
CEMES/CNRS, 29, rue Jeanne Marvig, 31055 Toulouse Cedex 4, France

P. Delhaès
CRPP/CNRS, Avenue Dr Albert Schweitzer, 33600 Pessac, France

(Received 1 October 2001; accepted 11 April 2002)

Chemical vapor infiltration (CVI) has been widely studied under several conditions to obtain C/C composites. A “film boiling technique” (so-called Kalamazoo), by the use of liquid precursor, based on thermal gradient CVI has been recently developed as one of the very effective techniques to increase the carbon yield and the densification rate. A small cold wall type laboratory reactor has been realized to analyze the kinetics of reactions and the deposited pyrocarbon matrix. In this study, ferrocene, as the source of catalyst, is mixed to the liquid precursor to induce a catalytic effect on the film boiling technique since the transition metals are known to increase the carbon deposition rate. In addition to an important increase of the densification rate, it is revealed that the deposition mechanism and microtextures are completely modified by the presence of catalyst, with the presence of multiwall nanotubes within the matrix. A model has been adapted from Allendorff and Hunt’s work to interpret this peculiar deposition mechanism.

I. INTRODUCTION

The C/C composites have been studied as very useful structural materials because of their thermal shock resistance due to high thermal conductivity and low thermal expansion, in addition to their mechanical properties such as high strength, toughness, and stiffness. To combine a porous fibrous preform with a carbon matrix acting as a binder between the fibres, the most widespread method to obtain the C/C composite is the isothermal chemical vapor infiltration (CVI) process. Gaseous hydrocarbons are used as precursors, which lead to the deposition of carbon matrix, in a competition between pyrolysis chemical reactions and diffusion of the chemical species inside the porous preform.

Thermal gradient CVI processes using cold wall reactors overcome diffusion limitations and increase the infiltration rate, giving shorter processing times.¹ More recently, a fast densification process, based on a film boiling technique and so-called “Kalamazoo,” has been developed.² It is based on a very strong thermal gradient created—by inductive or resistive Joule effect—between the central part of the heated fibrous preform and its peripheral part immersed in the liquid hydrocarbon precursor. The well-known results for the deposited matrix are respectively a very high rate of densification with an

improved carbon yield, a very low residual porosity, and a “good” matrix quality. The usual matrix microtextures are observed in specific anisotropic pyrocarbons, called smooth laminar and rough laminar; the second one, known for being graphitizable, is the most useful for applications.³

One effective factor to modify the deposition way and the infiltration kinetics of CVI is the catalytic effect which gives birth to a new process family: the catalytic chemical vapor infiltration, CCVI.¹ Many previous studies showed that small particles of transition metals such as Fe, Ni, or Co have significant effect on the control of the nucleation and growth characteristics of carbon^{4,5} and thus enhance appreciably the carbon deposition rate from hydrocarbons.⁶ The principle of this effect is attributed to carbon diffusion through the catalytic particles, which promotes gas decomposition. It has already been revealed that precursor gas decomposition occurs on these metal particles at lower temperatures than on regular carbon substrates.⁷ In addition, the catalyst particles reaching the heated surface increase the density of available nucleation sites, which promotes the rapid matrix deposition.⁸ CCVI is sensibly influenced by several experimental parameters such as catalyst particle size and nature of the transition metal, which modify the process for the carbon formation.

In a previous comparative study with small laboratory reactors,⁹ *in situ* and *ex situ* experiments have been carried out with various liquid carbon precursors to analyze both the kinetics of deposition and the carbon yield with the film boiling technique.

In this study, we use the same experimental setup as previously described. Mixed with cyclohexane as the liquid carbon precursor, ferrocene (dicyclopentadienyliron: $C_5H_5-Fe-C_5H_5$) is introduced as a source of iron to investigate the catalytic effect on the carbon formation. We then present the physical and structural characteristics of the deposited matrices under various conditions. All polyaromatic carbons are multiscale materials. They are described by different levels of organization. In order to complete the microscale observation performed by optical microscopy and to be able to discuss about the catalytic CVI mechanism, it is necessary to get a deeper insight at the nanometer scale.¹⁰ In a detailed transmission electron microscopic (TEM) study, we will show that under these catalytic conditions different nanoparticles are also synthesized. This fact led us to propose a chemical mechanism for this process, based on a moving reaction front.

II. EXPERIMENTAL SETUP

In the boiling film technique, the heated porous substrate or preform, is immersed directly into a liquid hydrocarbon as the source of carbon. The hydrocarbon is vaporized by the calefaction effect and then cracked so as to produce the carbon deposit at the contact with the inner hot substrate. A mobile deposition front starts to move from the core toward the preform surface. In this method, a very strong thermal gradient, as opposed to the gaseous conventional processes, is produced in the system because the liquid phase surrounding the preform keeps the outside temperature at its own boiling point.

A schematic illustration of the experimental setup is shown in Fig. 1. The cylindrical carbon preform ($\Phi = 2$ cm, $L = 4.5$ cm) is made of ex-cellulose carbon felt disks (RVC 2000 from Le Carbone-Lorraine Co., Courbevoie, France⁹) of an apparent density of 0.1, stacked around a central graphite rod ($\Phi = 3$ mm) resistively heated by Joule effect. This preform is placed vertically in the axis of the reactor.

The reference temperature of the sample is measured in the axial channel of the heating rod with an S-type thermocouple, fixed at the middle height of the preform and protected against carbide formation. The axial thermal gradient, measured by moving the thermocouple along the axis of the sample,¹¹ is lower than $5^\circ\text{C}/\text{mm}$. But the key thermal parameter is the radial gradient. As shown in Fig. 2, the radial temperature distribution inside the preform, measured once with a set of sleeved thermocouples (placed at 1 and 3 mm, respectively, from the graphite rod) is a function of the distance from the axial

rod during the CVI experiment. As the densification proceeds, the hot volume of highest temperature extends toward the external part, following the densification front. This result corresponds well to that measured by Bruneton *et al.*,² with an inductive heating: this means that the same principle governs both reactors.⁹

The ferrocene is diluted in cyclohexane in the range 0.1 to 5 wt%. The quantity of liquid mixture to completely immerse the carbon preform is poured into the reactor. The central graphite rod is heated by Joule effect at constant temperatures of 900, 1000, 1100, and 1200°C , respectively.

Because the temperature of the liquid phase could be kept during the experiments at its boiling point ($T_B = 80^\circ\text{C}$ for pure cyclohexane), the thermal gradient is

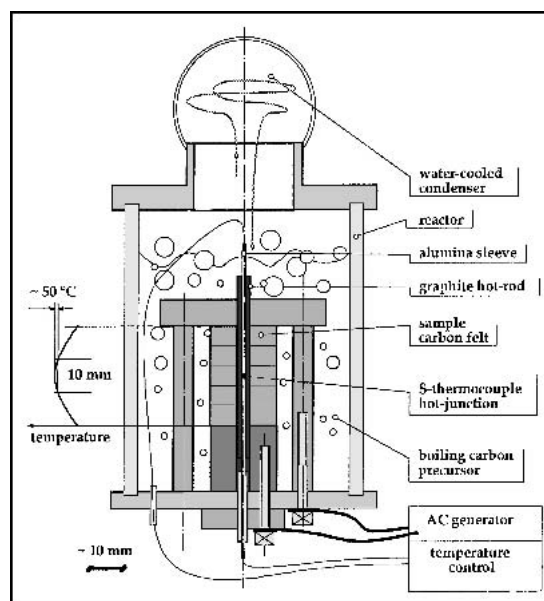


FIG. 1. Schematic experimental setup showing the axial temperature profile.

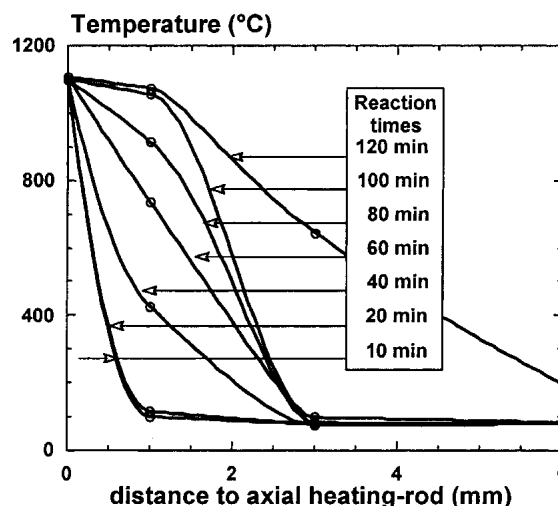


FIG. 2. Radial temperature profiles in the sample for increasing times in absence of catalyst.

reaching about 300 °C/mm along a radius of the sample. A deposition time of 30 min is kept constant for all the experiments. A comparative study in the presence or not of ferrocene in cyclohexane is carried out and presented in the following.

III. EXPERIMENTAL RESULTS

As in previous studies, we examine the quantity of deposited matrix, the deposition rate, and then the related textural and structural features including graphitizability and also the final iron content inside the matrix.

A. Matrix formation

The variation of the mass of deposits versus the initial ferrocene concentration in the liquid precursor is shown in Fig. 3. A maximum rate has been obtained at 1000 and 1100 °C with 0.5 wt% ferrocene. It is interesting to note that in absence of ferrocene there is no carbon deposit under 1000 °C, whereas at 1200 °C the catalytic effect does not appear to be so crucial. With an increased concentration of ferrocene, the mass of deposit tends to decrease slightly in the temperature range 1000 to 1100 °C.

The density of the composite is around 2.5 (obtained from He-pycnometry using a Micromeritics AccuPyc-1330, Norcross, GA), exceeding the usual values for carbon composites. This, combined with the magnetic behaviour of the samples, shows off the composition of the deposited matrix which must contain a certain amount of iron-containing particles. To determine this average concentration, composite samples have been heated up to 600 °C for 2 h in an open furnace. The quantity of iron is calculated from the resulting mass of iron oxide (i.e., Fe₂O₃ in principle).

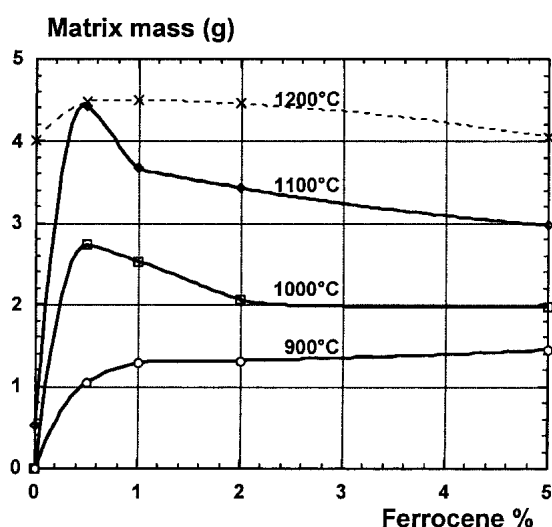


FIG. 3. Mass of deposited matrix as a function of the initial ferrocene concentration in the precursor.

The iron/carbon atomic ratio (Fe/C) in the deposited matrix depends on the same ratio in the liquid phase as shown in Fig. 4. This ratio is at least ten times larger in the deposit than in the pristine solution. In addition, the concentration of iron included in the deposits obtained at 1100 °C is about twice as much as at 1000 °C. It is thus demonstrated that pyrolysis of ferrocene is faster than cyclohexane leading to a depletion of catalyst in the mobile phase.

Indeed we must note that the transition metal whose catalytic effect is studied here is not recovered but trapped in the material it helps to produce and that its vector (ferrocene) is destroyed, in contradiction with a fundamental characteristic of regular catalysis (see Sec. III.D).

B. Deposition rate and densification front

The observation of a cross section of a composite sample by optical microscopy (Fig. 5) shows what we have called a densification profile,⁹ related to the evolution of the temperature distribution as presented in Fig. 2. It is composed schematically of three concentric zones from the center: (i) a (more or less) fully densified zone, with a residual closed porosity; (ii) a densification front with an open porosity; (iii) a nondensified zone, working only as a thermal and mass exchanger, heating up the precursor flow (calefaction phenomenon).

The two factors necessary to understand the experimental densification profile, are respectively the deposition and the densification rates. The deposition is the basic process that leads to densification of a porous matrix; this deposition rate is measured by the increase of the deposited matrix thickness around each individual fiber of the preform.¹¹

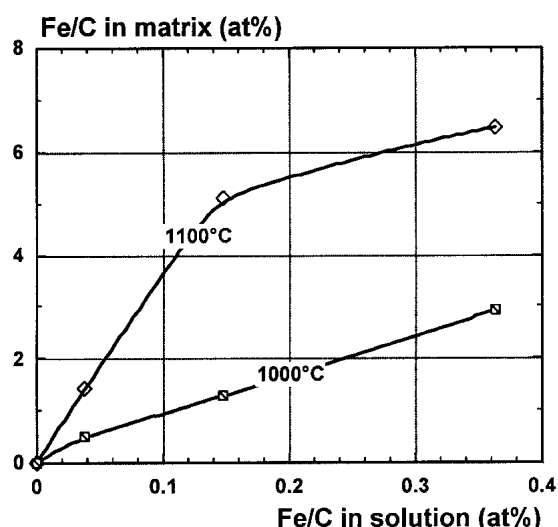


FIG. 4. Relation between the iron/carbon atomic ratios in the solution and the deposit, at two deposition temperatures (T_D).

The densification rate is measured from the radial thickness of sample that looks completely densified across a section of the sample. Figure 5 shows how this densification rate is determined by optically measuring the thickness of the pyrocarbon deposited around the single filaments. As a function of the initial ferrocene concentration in the liquid precursor, it is largely increased by the presence of catalyst, reaching a value of about 10 mm/h at 1100 °C.

Qualitatively, the aspect of the composite (Fig. 5) is very different from what we observe in the absence of catalyst.⁹ Two points are thus evidenced: (i) With catalyst, there is practically no residual porosity at a micronic scale, and we can only calculate an equivalent deposit thickness (curve A) from the average half distance between two carbon fibers. Without catalyst, we can actually draw the deposition profile (curve B) from the individually measured deposit thickness. (ii) The deposition front, with catalyst, is very sharp, indicating a completely different chemical mechanism.

The densification in the presence of catalyst thus appears to be faster and more complete. A change in temperature profile and temperature evolution with time is also observed, due to the presence of catalyst (Fig. 6). To understand this, we measured with a thermocouple the axial reference temperature (curve A), and then with

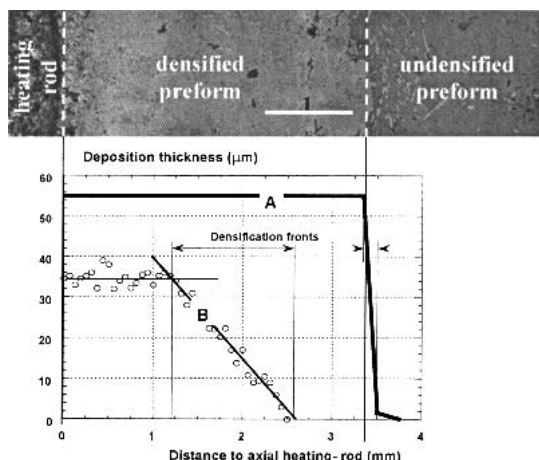


FIG. 5. Densification profile observed by optical micrography of a cross section of the composite ($T_D = 1000$ °C; ferrocene in cyclohexane = 0.1 wt%): (A) associated densification profile in presence of catalyst; (B) for comparison, without ferrocene.

two other thermocouples inserted at two different distances inside the preform, respectively 1 mm (curves B and D) and 3 mm (curves C and E) from the central heating rod, we measured the radial temperature with catalyst (curves B and C) and without (curves D and E). In the presence of catalyst, the temperature rise starts earlier than in absence of catalyst for both thermocouples. Two reasons are to be considered to explain this change of temperature profile by the catalyst: a modification of the thermal conductivity of the matrix due to the deposition chemical mechanism and the presence of iron particles.

C. Microtexture observation by optical microscopy

Polished surfaces of the samples are observed by optical microscopy under polarized light between crossed polarizers. An optical activity, due to the birefringence of graphitic carbon domains, is relevant to the presence of large (in the micronic range) oriented sp^2 domains as in SL or RL type microtextures usually found under both isothermal and “Kalamazoo” conditions.^{9,12,13}

The obtained microtextures are summarized in Table I for deposition temperatures $T_D = 900, 1000,$ and 1100 °C and initial catalyst concentration between 0 and 5% in weight.

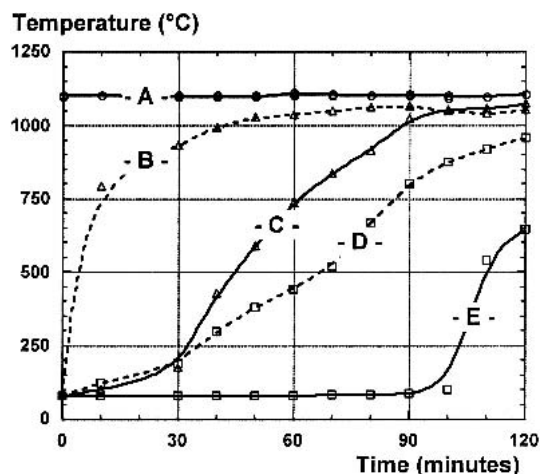


FIG. 6. Temperature evolutions inside the sample ($T_D = 1100$ °C): (A) reference axial temperature; (B) at 1 mm from the heating rod with catalyst; (C) at 3 mm from the heating rod with catalyst; (D) at 1 mm from the heating rod without catalyst; (E) at 3 mm from the heating rod without catalyst.

TABLE I. Matrix microtextures under various experimental conditions (as seen by optical microscopy).

Temperature	Ferrocene					
	0%	0.1%	0.25%	0.5%	1%	5%
1100	Anisotropic	Isotropic and anisotropic	Isotropic and anisotropic	Isotropic and anisotropic	Isotropic	Isotropic
1000	No deposition	Isotropic	Isotropic	Isotropic	Isotropic	Isotropic
900						

In the presence of any amount of iron, the mostly represented microtexture of the matrix looks completely isotropic as defined by the absence of any bright area. It is the only kind of matrix observed with ferrocene at 900 and 1000 °C and, in the case of initial ferrocene concentration from 1% and beyond, at 1100 °C. At this high temperature and for ferrocene concentration under 1%, we find well-defined areas where anisotropic matrix is deposited, looking like the RL microtexture normally observed at 0%.⁹

In fact, at any temperature, deposition starts under “catalytic conditions,” giving a matrix containing iron particles with specific characteristics, particularly optical isotropy. Then, as a consequence of the pyrolysis kinetics of ferrocene, faster than that of cyclohexane, when temperature is high enough (>1100 °C) and initial ferrocene concentration low enough (<1%), there may be in some restricted areas a lack of catalyst leading to carbon deposition in “out of catalyst” conditions. Figure 7 shows such an area where carbon fibers are covered first by an isotropic matrix layer and then by an overlay of a classical anisotropic laminar pyrocarbon.

D. Iron concentration by electron probe microanalysis (EPMA)

This method has been used to reveal the precise distribution of the iron included in each part of the composite samples. Giving at the same time for the same point an image of the sample and the distribution of iron (Fig. 8), this method is an accurate tool to determine the relation between the microtexture and the concentration of iron.

Figure 9 shows this distribution inside the isotropic phase obtained in the early deposition time at the contact with the heating graphite rod at 1000 °C with an initial

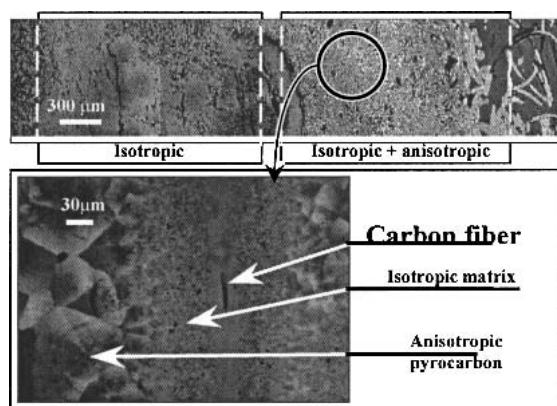


FIG. 7. Optical micrographs of superimposed isotropic and anisotropic microtextures ($T_D = 1100$ °C; ferrocene in cyclohexane = 0.1 wt%).

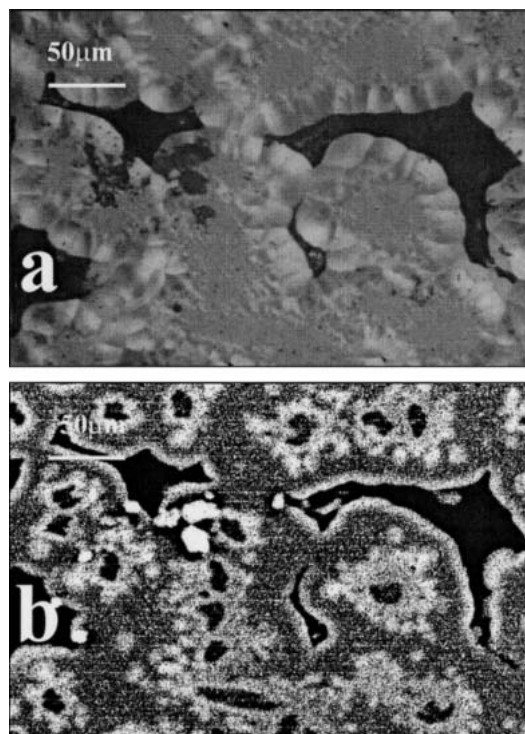


FIG. 8. Images of a composite sample ($T_D = 1100$ °C; ferrocene in cyclohexane = 0.5 wt%): (a) by optical microscopy; (b) by E.P.M.A. of iron.

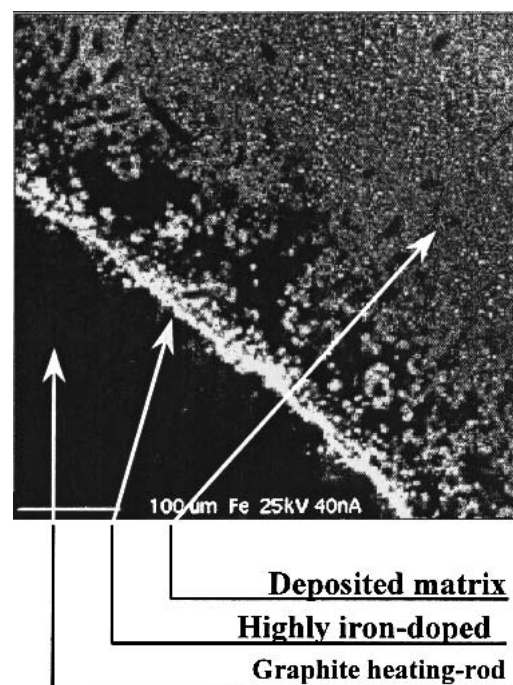


FIG. 9. E.P.M.A. of iron in a sample ($T_D = 1000$ °C; ferrocene in cyclohexane = 0.1 wt%).

ferrocene concentration of 0.1%. Iron particles appear in white in this picture. A very high concentration of these particles is detected at the boundary between the deposit and the graphite heating rod, showing that deposition begins with the pyrolysis of ferrocene on the hot surface.

The presence of seed particles is reported to promote carbon deposition⁸ by increasing the available density of nucleation sites on the substrate. It helps carbon nucleation that cannot easily occur on the graphite substrate at low temperature. It can be thought as one reason the temperature close to the graphite heating rod increases rapidly, as shown in Sec. III.A.

It also reveals that the concentration of iron included in deposits depends on their structure. Figure 8 shows the concentration of iron [Fig. 8(b)] in each texture revealed by its optical microview [Fig. 8(a)]. It is confirmed that iron is concentrated in the isotropic matrix areas and then in a thin layer on the surface of the anisotropic pyrocarbon (probably as ferrocene adsorbed at low temperature at the end of the experiment). Indeed iron concentration inside the usual anisotropic pyrocarbon is very low.

E. Graphitization process

Graphitizability is a very interesting property for the thermostructural applications of carbon/carbon composite materials. This is checked by x-ray diffraction analysis of samples before and after a high temperature treatment (HTT) for 90 min at 2500 °C. For example the isotropic microtexture ($T_D = 1100$ °C with 5% of ferrocene) analyzed before HTT has no measurable value for d_{002} but is 3.365 Å with a full width half-maximum value of 1.15° after thermal treatment. This sharp 002 diffraction peak shows that this isotropic phase behaves as a RL pyrocarbon microtexture which is the only graphitizable one, i.e., evolving toward the thermodynamically stable phase of hexagonal graphite.¹⁰ This rather surprising result has incited us to carefully examine this “isotropic” matrix.

F. TEM observations

Since the pyrocarbon deposited by the “Kalamazoo” method normally exhibits anisotropic microtexture,^{9,11} the catalytic effect of iron is to modify the matrix microtexture to an isotropic one. To reveal the real texture, nanoscale observations have been carried out by TEM.

Two samples ($T_D = 1100$ °C with respectively 5 and 0.5% of ferrocene mixed with cyclohexane) are prepared by gentle grinding then deposited on a lacey carbon grid. Both were investigated using a Philips EM400 TEM equipped with a high-resolution stage and operating at 120 kV (point resolution = 3 Å).

The morphology, texture, and size of the various pyrocarbon deposits strongly depend on that of the catalytic particles, as shown on the first sample (ferrocene 5%).

The latter corresponds to black parts in Fig. 10 with a size distribution from 5 to 200 nm. The deposits present different shapes and mainly three kinds of morphology are observed; in all cases, the carbon growth occurred from the particle surfaces. Figure 10(a) corresponds to a bifilament, where the growth of carbon started from the surface of a catalytic particle with a square shape, in two opposite directions. Figure 10(b) shows a boundary between the particle and the initial deposit; it can be seen that the aromatic layers are formed along the particle surface so that graphenes are oriented parallel to the crystal face. Figure 10(c) shows concentric multiwall shells

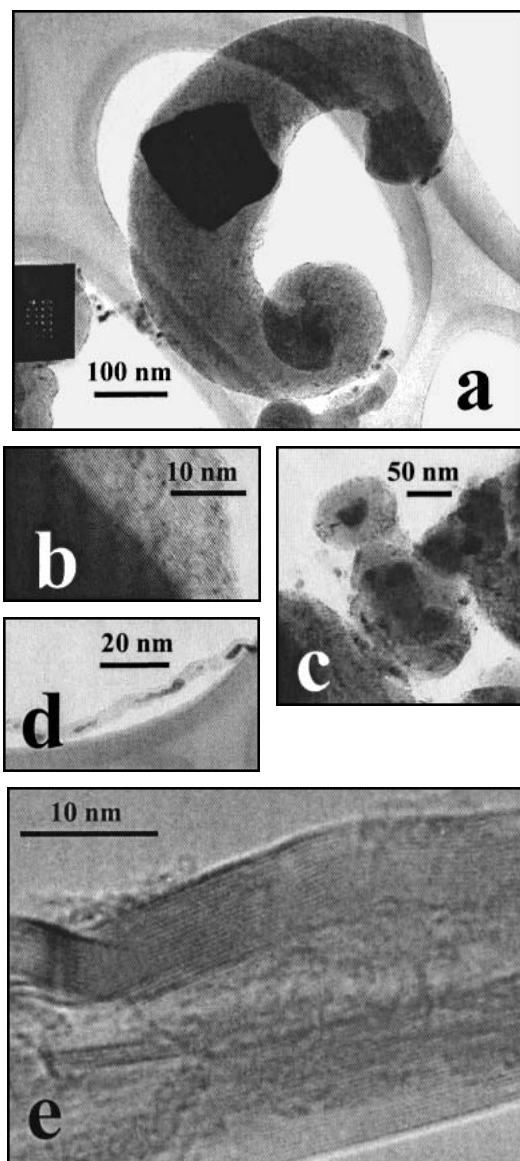


FIG. 10. TEM bright-field images of various shapes found in the sample composite ($T_D = 1100$ °C, ferrocene in cyclohexane = 5 wt%): (a) carbon bifilament growing from a catalyst particle; (b) carbon/catalyst particle boundary; (c) multiwall shells carbon growth around round shaped catalyst particles; (d, e) carbon nanotube.

deposited around the particles, especially when exhibiting round morphology. In the latter case, tubes and filaments are not formed since the growth does not follow specific directions. Figure 10(d) exhibits a carbon nanotube, inside of which normally many small particles are placed. The observed tubes have a diameter of 10 to 50 nm and a length around 1 μm . Figure 10(e) shows the walls of such tubes constituted of long and straight parallel aromatic layers with a continuous length of more than 100 nm.

On the second sample (ferrocene 0.5%), although the densification remains uncomplete at low scale, with an open porosity likely to induce a poor fiber/matrix adhesion [Fig. 11(a)], a lower ferrocene amount gives rise to a higher compactness at high scale [Fig. 11(b)]. Correspondingly, nanofibrous morphologies such as that of Figs. 10(a) and 10(d) are not evidenced. Local textures are most often concentric, generally around “catalyst” particles. Their porosity is rather low but increases locally when increased anisotropic display of graphenes occurs [Fig. 11(c)]. It is worth noting that the bulk textural aspect of the deposited matrix may somewhat resemble that of a carbonized, heterogeneous petroleum

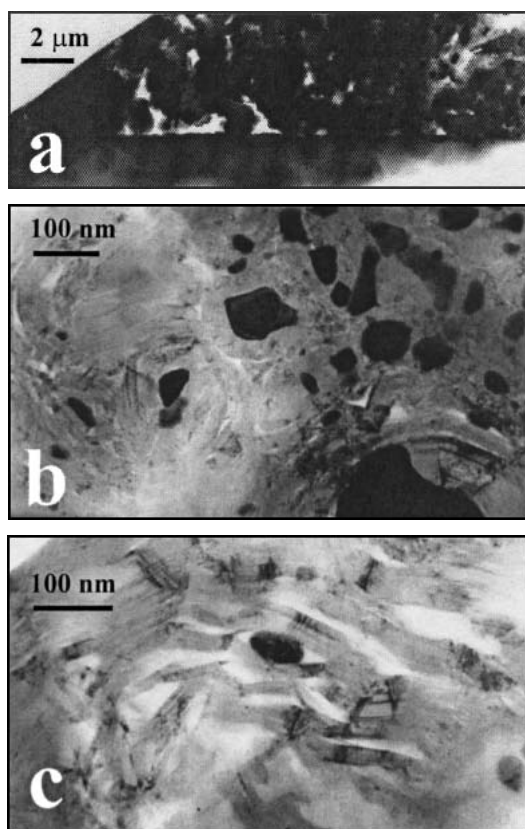


FIG. 11. TEM bright-field images of the sample ($T_D = 1100\text{ }^\circ\text{C}$, ferrocene in cyclohexane = 0.5 wt%): (a) low scale of the deposited matrix at the fiber contact; (b) concentric texture-rich area of the matrix; (c) anisotropic textured area of the matrix.

pitch like those used for the liquid impregnation of fibrous preforms and the subsequent preparation of carbon/carbon composites.

Such features, good nanotexture and polyhedral graphene stacks, are found for temperatures far beyond 2000 $^\circ\text{C}$ for heat-treated liquid carbon precursors without catalyst.¹⁴ The structure is turbostratic (Fig. 12) although diffraction rings ($hk0$) appear sharp, i.e., no hkl diffraction ring is found ($d_{002} \approx 0.344\text{ nm}$), and becomes completely graphitizable under further treatment as just described (see Sec. III.E). As already shown,^{15,16} this is related to the presence of catalyst inside the matrix.

From TEM observations, it has been revealed that a variety of carbon deposits in the so-called “isotropic” phase always starts from the surface of the catalytic particles. Although the temperature of 1000 $^\circ\text{C}$ is high enough for the usual formation of carbon deposits in catalyst-free conditions,⁹ no “isotropic” pyrocarbon has been observed starting from the deposition on a carbon fiber surface. The deposition mechanism starts from the seed particles which are supposed to be transformed at a lower temperature in cementite (Fe_3C) by dissolution of carbon within iron.^{17,18}

To summarize, our experimental conditions have led to the formation of different types of carbon nanoparticles all mixed up. In particular, for a high content of ferrocene, multiwall nanotubes are obtained inside this confined volume following an already described catalytic way for nanotubes formation.^{15,19}

IV. PROCESS MECHANISMS

A. Discussion about the deposition mechanism

The catalytic effect is due to the iron introduced during the formation of the matrix by decomposition of the ferrocene molecules. It allows much higher amount of deposit starting at a lower temperature (900 $^\circ\text{C}$) compared to classical CVI. This is confirmed by a kinetics analysis;

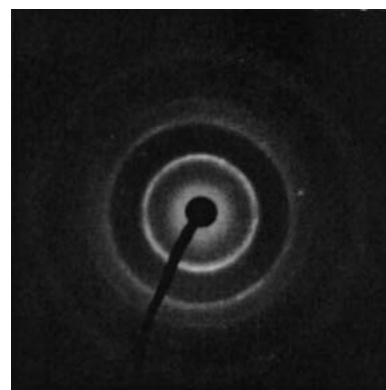


FIG. 12. Electron diffraction pattern from the deposited matrix in “catalytic” conditions. The most intense ring is 002, corresponding to $d \sim 0.344\text{ nm}$.

from the Arrhenius plot, it is deduced that the densification rate is practically exponential with the reaction temperature. As shown in Table II, the apparent activation energy (E_A) values obtained in presence of catalyst are around 70 kJ/mol, which is very low compared to the value for the densification in the absence of catalyst as determined by Bruneton *et al.*² $E_A = 222$ kJ/mol. It shows that the deposition mechanism in the presence of catalyst is different with a faster kinetics constant which overbalances the usual one. Indeed the formation of an “isotropic” phase obtained by catalytic effect easily occurs and is not strictly limited by lower temperature conditions, as compared to the usual pyrocarbon deposition.

The presence of catalyst modifies the deposition mechanism and therefore the carbon microtexture which results in an improvement of the densification rate. Normally the pyrocarbon deposition occurs around each fiber of the preform without catalyst.⁹ In the presence of catalyst, the matrix deposition can be considered to occur on the surface of seed particles in vapor phase as in classical supported catalysis (Fig. 13), associated to a modification of the temperature gradient.

B. Model for the densification process

Our experimental results have shown that a catalytic effect is present which allows an infiltration process at lower deposit temperatures to be obtained with a weight uptake multiplied by 5 at $T_D = 1100$ °C (Fig. 3) as demonstrated by the lowering of the apparent activation energy E_A (Table II). To explain this behavior we consider both the mechanisms and kinetics of CCVI process by taking into account a model for particle–vapor codeposition.²⁰ Its optimization, as evidenced Fig. 3, should be related to the inlet of precursor gas inside the preform and the codeposition mechanism.

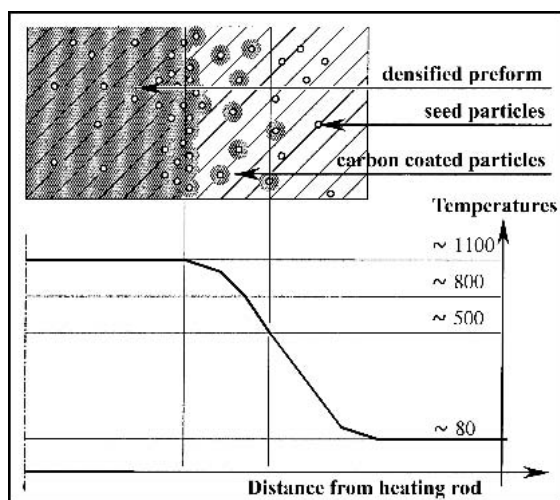


FIG. 13. Deposition model with catalytic seed particles and correlated temperature profile.

(i) As we have seen from the observation of the thermal gradient (Fig. 6), the catalytic effect is active in promoting carbon deposition at a much lower temperature (around 500 °C) than for classical CVD processes. We can assume from our TEM experiments that, in a first step, transition metal particles are formed and then, due to the presence of a reductive atmosphere, cementite-like grains may be formed from them during the pyrolysis of the precursor mixture.^{21,22}

In a second step, the growing of carbon nanoparticles is occurring as described for example by Tibbets.²³ From our experiments we cannot describe the mechanism in details, but as shown by our TEM and optical microscopy observations of the matrix, we have found different types of particles, like concentric shells and filaments, as already noticed by McAllister and Wolf²⁴ in carbon/carbon composites. Nevertheless all these composites are not presenting high mechanical properties useful for structural uses, but due to their specific properties such as graphitizability and ferromagnetism,²⁴ they may be useful in other applications as, for example, thermal protections.

(ii) From the mechanism analysis we can infer the increase of the deposition rates by a particle–vapor codeposition. Hurt and Allendorf²⁰ have developed a CVD model applied for deposition of silicon carbide which leads to a growth rate enhancement characterized by the definition of a volumic deposition rate (dV/dt) as

$$dV/dt = (dV/dt)_{CVD} + (4/3 \pi R^3) F/G \quad , \quad (1)$$

where the first term is defined for the classical CVD process characterized by a deposition rate G in a kinetics-controlled regime in absence of catalyst. The second term is related to seed particles which are supposed to be spheres of radius R ; they are deposited at the interface with a rate F which characterizes a sticking coefficient of products and a rather sharp reacting front. Indeed the second term defines the enhancement factor related to the fine particle deposition on the substrate that we suppose here to occur following the described catalytic mechanism. Indeed, this model accounts for seed particles which are injected inside a hot wall reactor, therefore corresponding to different chemical and thermal conditions. This model of competing codeposition is however useful to understand that through two chemical ways with two different kinetics constants which work in different parts of the reactor because of the thermal gradient, a higher deposition rate is finally observed (Fig. 13).

(iii) As we have already described,⁹ this fast densification process of a porous preform is specific and characterized by a competition of mass and heat transports in the presence of a steep thermal gradient associated with interfacial chemical reactions.

TABLE II. Apparent activation energies, E_A , rate constants, k , and densification rate in function of the ferrocene concentration [Arrhenius law: $k = A \exp(-E_A/RT)$].

Ferrocene (wt%)	E_A (kJ/mol ⁻¹)	k (10 ³ g/h)	Densification rate (g/h)			
			900 °C	1000 °C	1100 °C	1200 °C
0.0	222 ²
0.5	73.9	4.9	2.12	5.60	8.92	9.68
1.0	83.7	15.2	3.24	5.14	7.60	20.43
2.0	63.7	2.5	4.04	5.44	6.26	14.22

Even if a global modeling is out of the current ability, two interesting points can be indicated. As we have shown, the molecular diffusion mechanism is still efficient in absence of catalyst.⁹ Using the Knudsen number (Kn),²⁵ which is characterized by the ratio between the mean free path of involved molecules and the pore diameters, two situations are recognized: (a) $Kn < 2$ is the diffusion regime where the Fick coefficient is predominant as the usual situation for small molecules.⁹ (b) $Kn > 1$ is the ballistic regime where the Knudsen process is important. The mean free path of molecules is inversely proportional to the square of the molecular diameter.

A rough calculation shows immediately that the observed catalytic nanoparticles are in a ballistic regime. Indeed, after their chemical formation in the gas phase, they stick directly to the surface and they form a straight wall as already observed by optical microscopy (Fig. 5).

A complementary point concerns the coupling between the chemistry and the thermal gradient. As we have observed, the thermal gradient is not so steep in the presence of ferrocene (Fig. 7). This is related to the catalytic effect which is starting around 500 °C; when the nanoparticles are formed, the thermal exchange inside the preform as well as the hot CVD region profile (i.e. above 1000 °C) are dramatically lowered when the catalytic effect is dominant. This is the reason, following the Hurt and Allendorf's model,²⁰ we can rapidly change from one regime to the other and, in consequence, from isotropic to anisotropic microtexture.

V. CONCLUSIONS

We have developed a bench reactor for studying a fast densification process in the presence of the catalytic effect given by the addition of ferrocene in the liquid precursor. This effect has been evidenced with the matrix deposited below 1000 °C and an increase of the deposition rate in the usual temperature range for making C/C composites. Indeed we have shown that the addition of 0.5% in weight of ferrocene to the carbon precursor (cyclohexane) gives rise to an optimized mass uptake at $T_D = 1000$ and 1100 °C. This catalytic process transforms also the texture of the deposited matrix from long-range to short-range anisotropy, appearing as isotropic at the optical microscopy resolution level.

We have also demonstrated that classical long-range anisotropic pyrocarbons may be deposited around this isotropic phase obtained for an early deposition time. Thanks to the microprobe analysis we have clearly shown that this morphological change is due to the presence and then the lack of iron-containing nanoparticles. This observation is evidencing clearly that the nucleation and growth mechanisms are modified in the presence of iron with two major consequences.

(1) First, the type of matrix is clearly modified with the presence of filaments and nanotubes of carbon as demonstrated by TEM observations; this mechanism has been explained qualitatively thanks to a particle–vapor codeposition process. The obtained composites seem however fragile with a smaller mechanical resistance than classical ones. However it is known that submicronic carbon filaments are useful fillers for composite materials.²⁶ The key point to progress in this direction would be to control *in situ* the filament production for reinforcing the matrix.

(2) Second, this catalytic mechanism appears very interesting with the formation of particles in the gas phase at a lower temperature which modifies the thermal gradient and, therefore, their thermal history.

We infer that the transport properties of heat and mass in porous media, which are two orders of magnitude larger than in isothermal CVI process, are the keys to understanding these fast densification processes.

These experiments show clearly that there is a coupling between the chemical and thermal processes inside the densification front: their accurate control may lead to various and useful composite materials.

REFERENCES

1. I. Golecki, *Mater. Sci. Eng.* **R20**, 37, 124 (1997).
2. E. Bruneton, B. Narcy, and A. Oberlin, *Carbon* **35**, 1593 (1997).
3. P. Delhaès, in *EURO-CVD II*, edited by M.D. Allendorf and C. Bernard (Electrochemical Society Proceedings **97-25**, Pennington, NJ, 1997), pp. 486, 495.
4. R.E. Zielinski and D.T. Grow, *Carbon* **30**, 925 (1992).
5. N.M. Rodriguez, A. Chambers, and R.T.K. Baker, *Langmuir* **11**, 3862 (1995).
6. P.A. Tesner, in *Chemistry and Physics of Carbon*, edited by P.A. Thrower (Marcel Dekker, New York, 1984), Vol. 19, Chap. 2.

7. S.D. Robertson, *Carbon* **8**, 365, 374 (1970).
8. M.D. Allendorf, R.H. Hurt, and N. Yang, *J. Mater. Res.* **8**, 651 (1993).
9. D. Rovillain, M. Trinqucoste, E. Bruneton, A. Derré, P. David, and P. Delhaès, *Carbon* **39**, 1355 (2001).
10. J. Goma and A. Oberlin, *Carbon* **24**, 135 (1986).
11. D. Rovillain, Ph.D. Thesis, Bordeaux I University, Bordeaux, France (1999).
12. H.O. Pierson and M.L. Liberman, *Carbon* **13**, 159 (1975).
13. X. Bourrat, B. Trouvat, G. Limousin, G. Vignoles, and F. Doux, *J. Mater. Res.* **15**, 42, 101 (2000).
14. M. Monthioux (unpublished results).
15. R.T. Baker, *Carbon* **27**, 315 (1989).
16. K.S. Kim, N.S. Rodriguez, and R.T.K. Baker, *J. Catal.* **134**, 253 (1992).
17. W.R. Ruston, M. Warzee, J. Hennaut, and J. Waty, *Carbon*, **7**, 47 (1969).
18. A. Oya and S. Otani, *Carbon*, **17**, 131 (1979).
19. H. Gaucher, Ph.D. Thesis, Orléans University, Orléans, France (1997).
20. R.H. Hurt and M.D. Allendorf, *AIChE J.* **37**, 1485 (1991).
21. R. Sen, A. Govindaraj, and C.N.R. Rao, *Chem. Phys. Lett.* **267**, 276 (1997).
22. N. Grobert, W.K. Hsu, Y.Q. Zhu, J.P. Hare, H.W. Kroto, B.R.M. Walton, M. Terrones, H. Terrones, P. Redlich, M. Rühle, R. Escudero, and F. Morales, *Appl. Phys. Lett.* **75**, 3363, 3365 (1999).
23. G.G. Tibbetts, M.G. Devour, and E.J. Rodda, *Carbon* **25**, 367 (1987).
24. P. McAllister and E.E. Wolf, *Carbon* **30**, 189 (1992).
25. S.K. Griffiths and R.H. Nilson, in *EURO-CVD II*, edited by M.D. Allendorf and C. Bernard (Electrochemical Society Proceedings **97-25**, Pennington, NJ, 1997), pp. 544, 551.
26. D.D.L. Chung, *Carbon* **39**, 1119 (2001).